PHYSICAL REVIEW B **83**, 064102 (2011)

Symmetry of ferroelectric phase of $SrTi^{18}O_3$ determined by *ab initio* calculations

M. Bartkowiak,[1,2,3] G. J. Kearley,[1] M. Yethiraj,[1] and A. M. Mulders[2,3]

[1]*The Bragg Institute, Australian Nuclear Science and Technology Organisation, Lucas Heights, New South Wales 2234, Australia*

[2]*School of Physical, Environmental and Mathematical Sciences, UNSW@ADFA, Canberra, Australian Capital Territory 2600, Australia*

[3]*Department of Imaging and Applied Physics, Curtin University of Technology, Perth, Western Australia 6845, Australia*

(Received 24 September 2010; revised manuscript received 10 January 2011; published 11 February 2011)

Substitution of more than 33% of the naturally abundant ^{16}O in strontium titanate $SrTiO_3$ by ^{18}O causes the system to become ferroelectric at low temperatures. The ferroelectricity has been observed via susceptibility measurements, but to date the details of the ferroelectric phase and the phase transition are unclear. Using *ab initio* density functional theory and lattice-dynamics calculations, we find that the stable structure of the ferroelectric phase is orthorhombic with *Ima*2 symmetry. The *Ima*2 point group is noncentrosymmetric and the proposed structure exhibits an electric dipole moment of (0.57 0 0) eÅ. The *Ima*2 symmetry is consistent with the limited structural details that are reported using neutron diffraction and Raman spectroscopy.

DOI: 10.1103/PhysRevB.83.064102 PACS number(s): 71.15.Mb, 77.84.−s

I. INTRODUCTION

Strontium titanate, $SrTiO_3$ (STO), possesses a range of interesting properties, and was the model system used for the first measurements of phonon soft modes. It also becomes a superconductor at millikelvin temperatures and can be a metallic conductor when chemically reduced.

STO is a quantum paraelectric[1] and its dielectric constant saturates at low temperatures because quantum fluctuations inhibit the transition[2] to a ferroelectric phase, and the evolution of the dielectric constant with temperature[3] is therefore arrested. Ferroelectricity in STO can be induced by applying an electric field[4] or by applying stress.[5] It was found[6] that STO becomes ferroelectric at low temperatures when the ^{16}O in STO is substituted with isotopic ^{18}O, and later it was shown[7] that this phase transition is observed when the fraction of ^{18}O exceeds 33%. The critical temperature increases with ^{18}O content, and when fully substituted with ^{18}O STO becomes ferroelectric at $T = 23$ K[6] and is denoted as STO18. It is postulated that the increased mass of oxygen lowers the frequency of lattice vibrations,[7] freezing the soft mode which would otherwise inhibit the ferroelectric phase transition in $SrTi^{16}O_3$.

Raman measurements confirmed the phase change by showing new peaks present in the low-energy region.[6] Neutron scattering experiments[8] showed that the new phase has a lower symmetry and is most likely orthorhombic. At present, the nature of the phase transition remains under debate, as nuclear magnetic resonance (NMR) results indicated an order-disorder mechanism,[9] while initial Raman experiments[10,11] suggested an ideal displacive transition resulting from softening of a Slater-like[12] ferroelectric mode. More detailed Raman experiments suggested that the transition is a soft-mode-type quantum phase transition involving the coexistentce of paraelectric and ferroelectric phases[13,14] or the percolation of polar clusters.[15,16] Raman experiments[17,18] indicated also that local symmetry-breaking regions appear at low temperatures in the crystals near the critical concentration of ^{18}O and these regions are precursors of the ferroelectric phase. It is theoretically possible[19] for the transition to combine displacive and order-disorder behavior.

Various theoretical models have been employed[20–23] to explain the phenomenon of the isotope-induced ferroelectric phase transition in STO.

The aim of the present study is to determine as many structural details as possible for low-temperature crystal structure of STO18 and to understand the mechanism of the transition.

Starting with the tetragonal unit cell, we performed density functional theory (DFT) calculations using Vienna *Ab Initio* Software Package (VASP)[24,25] to determine the total energy and optimize the crystal structure. We then used PHONON[26] to calculate the Hellman-Feynman forces, and thus the phonon dispersion curves and vibrational density of states. The phonon dispersion curves show that the tetragonal phase is unstable, and by following the atomic displacements of the imaginary mode we derived a stable and ferroelectric structure, *Ima*2.

II. METHOD

The procedure must start from a structural optimization that places the atoms in their potential-energy minima, making it possible to analyze the system dynamics using the direct method. This was achieved using the conjugate-gradient method for structural relaxation, this being the most robust procedure provided by VASP. In practice, different minimization algorithms usually affect the speed of convergence, but have little influence on the final outcome.

Clearly, when dealing with the energy calculations there is no difference between ^{16}O and ^{18}O, as the influence of the mass of the nucleus on the electronic configuration is not included in the pseudopotentials, but the increased mass of oxygen is included in the lattice-dynamics calculations.

In all the calculations performed with VASP, projector augmented wave (PAW) pseudopotentials[27,28] were used. The exchange correlation is included within the general gradient approximation (GGA) as implemented[29,30] by Perdew, Burke, and Ernzerhof (GGA-PBE). VASP uses Pulay mixing when updating the potential during the self-consistent calculation of the electronic ground state.

For the (2 2 2) supercells, the calculations have been performed with a $4 \times 4 \times 2$ Monkhorst-Pack shifted k-point mesh and 650 eV energy cutoff. The very high energy-cutoff

TABLE I. Summary of lattice parameters and atomic coordinates for structure A—the experimental structure of paraelectric $SrTiO_3$ at T = 1.5 K[32], structure B—the calculated structure of paraelectric $SrTiO_3$ obtained with VASP, and structure C—the calculated structure of ferroelectric $SrTiO_3$ obtained with VASP and PHONON. The lattice parameters and atomic coordinates of structure C have been transformed for ease of comparison with structures A and B. The actual *Ima*2 cell can be constructed only after changing the sequence of lattice parameters from (*a b c*) to (*c b a*) and the atomic coordinates from (*x y z*) to ($z + 0.25$ y $x + 0.25$).

Structure	A	B	C
Point group	$I4/mcm$	$I4/mcm$	*Ima*2
a [Å]	5.5134	5.5134	5.5043
b [Å]	5.5134	5.5134	5.5036
c [Å]	7.8072	7.8072	7.8341
Fractional coordinates			
O1	(0 0 0.25)	(0 0 0.25)	(−0.004 0 0.25)
O2	(0.2412 0.7412 0)	(0.2261 0.7261 0)	(0.7215 0.2247 0)
O3	–	–	(0.2722 0.2246 0.5)
Ti	(0 0 0)	(0 0 0)	(0.00224 0.00044 0)
Sr	(0 0.5 0.25)	(0 0.5 0.25)	(0.0008 0.5 0.25)
Number of atoms in the unit cell	20	20	20
Total energy [eV]	−160.573 019	−160.597 644	−160.599 194

is important for strain determination and therefore cell-shape optimization. This requires higher cutoff values than any other property calculated in the structure optimization process.

With PHONON the dynamical matrix was determined using the direct method,[31] and that is where the increased mass of oxygen was included. For each structure a (2 2 2) supercell was created and a minimal set of atom displacements necessary to obtain all elements of the dynamical matrix was determined. For each direction a positive and negative displacement was applied. The amplitude of displacement used in the calculations was 0.03 Å, which yields good results for most systems. A higher amplitude may decrease the accuracy of the results, as the harmonic approximation of the potential only holds within a limited range, while a lower amplitude limits the precision of the numerical approach due to rounding errors.

For each of the distorted structures, VASP was used to minimize the energy of the electronic system and determine the forces acting on the ions. All calculations were performed using the same set of parameters, as even a small change of energy cutoff or a modification of the *k*-point mesh may result in a change in the potential shape and therefore move the potential minima away from the atom positions. PHONON was used to determine the dynamical matrix from the forces, followed by the calculation of phonon dispersion curves and the vibrational density of states.

In addition, we performed molecular dynamics (MD) simulations, also using VASP. In each of the simulations we used a (3 3 2) supercell. The *k*-point mesh included the Γ point only and the energy cutoff was reduced to 300 eV. A time step of 1 fs was used, and each simulation run consisted of at least 6000 steps.

VASP implementation of Berry's phase formalism was used for the determination of the electronic dipole moment. Only a single unit cell was considered in each case using a *k*-point mesh of 8 × 8 × 8, and an energy cutoff of 650 eV. The number of *k* points was higher than for a (2 2 2) supercell because the volume of reciprocal space to be sampled is inversely proportional to the volume of the system.

III. RESULTS

The starting point of our DFT calculations is the tetragonal cell obtained by Kiat *et al.* using Rietveld refinement of x-ray diffraction data[32] (structure A in Table I). These experiments were performed at 1.5 K, which is advantageous for the DFT calculations that are formally at 0 K.

The cell parameters were fixed because the change in unit cell due to thermal expansion to 1.5 K is much smaller than the uncertainties of DFT. Our DFT relaxation process resulted in structure B (Table I). The symmetry of this structure remained tetragonal, with the $I4/mcm$ point group and displacements of atoms within the unit cell resulted in lowering of the total energy. In particular, the relaxation process increased the rotation angle of the TiO_6 octahedra as illustrated in Fig. 1.

PHONON was then used for calculating the dispersion curves and density of states, the former being illustrated in Fig. 2.There are significant imaginary frequencies present at theΓ point of the Brillouin zone, which indicates that structure B is not stable. By displacing the atoms along the directions associated with the imaginary mode the total energy of the system (Fig. 3), plotted against the average amplitude of atom

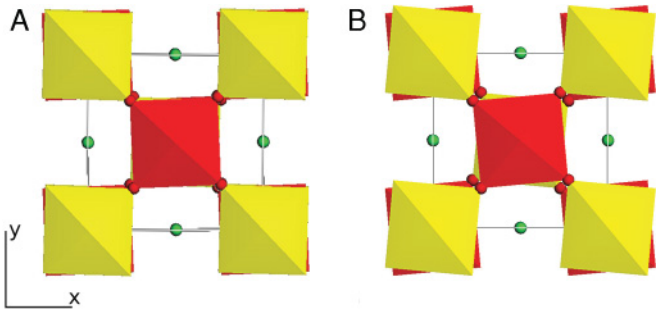

FIG. 1. (Color online) Illustration of the crystal structure of STO for the experimental structure A observed at 1.5 K[32] and the derived structure B obtained by minimizing the energy using VASP. Sr atoms are indicated with green and the TiO_6 octahedra are indicated in red and yellow. Note that the torsion angle of the TiO_6 octahedra is increased after relaxation.

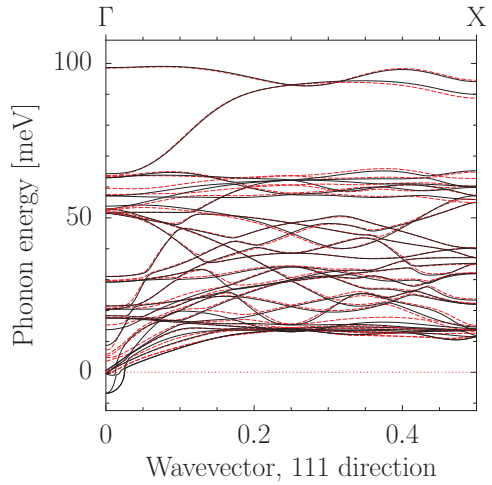

FIG. 2. (Color online) Phonon dispersion curves calculated for structure B (black lines) and structure C (dashed red lines) from the center the Briilloin zone to the zone boundary along the [111] direction. The negative values correspond to calculated imaginary frequencies. Structures B is not indicated by the imaginary phonon frequency at the the Γ point.

displacement) passed through a new lower minumum. Figure 4 shows the directions of atom displacement associated with the imaginary mode. The optimal average displacements are 0.024 Å for the oxygen atoms, 0.017 Å for the titanium atoms, and 0.005 Å for the strontium atoms. Even this structure is not optimized since the cell shape may change, so a further structural relaxation was made using a fixed unit cell volume, but allowing optimization of the cell shape, which resulted in an orthorombic cell with symmetry *Ima*2 (labeled C in Table I). We then used PHONON to obtain the phonon dispersion curves and the density of states of this new structure, C. (see Figs.2 and 5).

The Berry's phase formalism was used to calculate the ferroelectric moment of the three structures (see Table I). The electric dipole moment is zero for both structures A and B, while for structure C this is (0.57 0 0) eÅ.

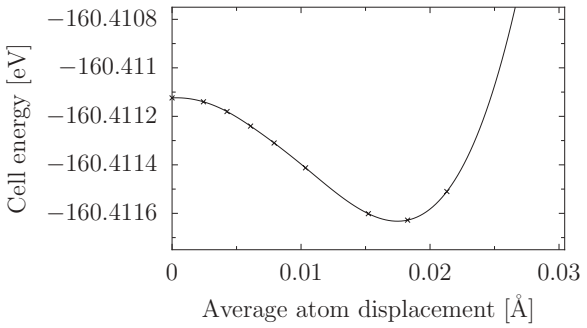

FIG. 3. Energy per unit cell plotted against the amplitude of atom displacement. The atoms are displaced along the directions associated with the imaginary frequency at the Γ point (see Fig. 4). The displacement amplitude varies between atoms and therefore the abscissae axis shows the average displacement per atom. The energy was calculated using (2 2 2) supercells and the energy values are lower than in Table I due to the difference in energy cutoff (see the methods section).

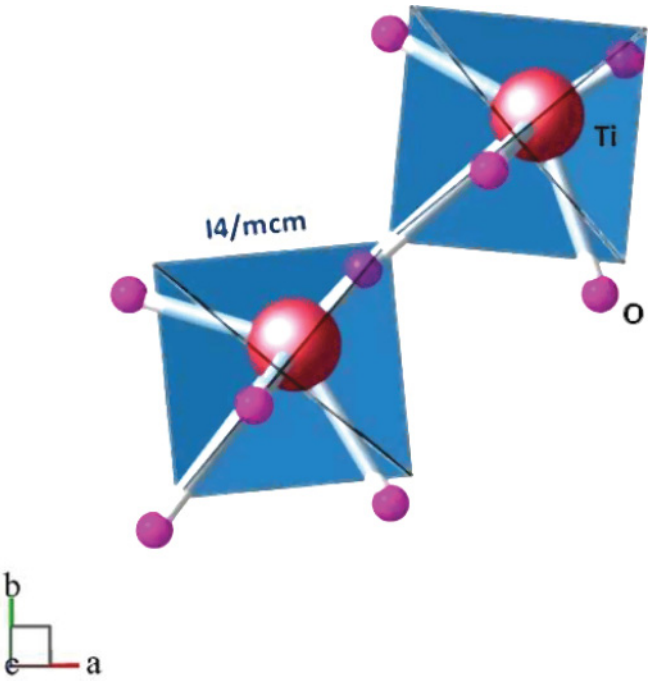

FIG. 4. (Color online) Illustration of the displacements associated with the imaginary phonon frequency at the Γ point compared to their equilibrium positions in $I4/mcm$ tetragonal structure B. The amplitude of the displacement has been multiplied by a factor of 20 for clarity. The instability leads to a Slater-like translation of oxygen atoms with respect to strontium and titanium positions. This picture was prepared with BALLS AND STICKS software.[33]

IV. DISCUSSION

Our initial relaxation of structure A to structure B resulted in a distinguishable difference, as illustrated in Fig. 1. This is probably because the experimental atomic positions correspond to the thermal average, while energy optimization places the atoms in the minimum of the potential. To test this possibility we performed MD simulations at 80 K and found that the time-averaged positions from this simulation are indeed closer to those determined by experiment. Clearly, dynamic effects play an important role in the structure STO. The experimentally observed structure resembles that obtained from our DFT calculations and exhibits larger thermal parameters than would be expected at this temperature. Structure B is unstable to the Slater-like phonon mode illustrated in Fig. 4. This instability leads to a lowering of the crystal symmetry from $I4/mcm$ to *Ima*2, which is noncentrosymmetric and can support a ferroelectric moment that we find to be (0.57 0 0) eÅ. This confirms that structure C is ferroelectric and qualitatively different from structures A and B.

Figure 2 illustrates the difference between the phonon dispersion curves of structures B and C. The increased stability of C is apparent as the lowest "negative" frequency at the Γ point is increased from −6.65 to −0.25 meV, this value being insignificantly different from zero for calculations of this type. The orthorhombic space group that we find, *Ima*2, is also in agreement with the neutron diffraction data of Noda *et al.*[8] who found that the space group of the ferroelectric phase should be one of $I4cm$, $Iba2$, $I2cm$, $Fm2m$, $F2mm$, or $Fmm2$.

TABLE II. Frequency of the Raman peaks observed by Shigenari *et al.*[34] compared to the calculated Raman frequencies for structure C. For Raman frequencies higher than 100 cm^{-1} the calculated frequencies match the experiment well. The first section of the table lists the phonon modes at the Γ point, and the second part the phonon modes from the zone boundary of the cubic phase, which appear at the Γ point due to folding of the Brillouin zone.

Observed Raman frequency[34] [cm^{-1}]	Assignment[34]	Calculated Raman frequency [cm^{-1}]	Assignment
17	A_1/B_2	47	B_2
17.5	B_1	42	B_1
171	A_1/B_2	167	B_2
171	A_1/B_2	167	A_1
171	B_1	174	B_1
517	A_1/B_2	510	B_2
		512	A_1
517	B_1	514	B_1
11	B_1	29	B_1
17.5	A_2	38	A_2
44	A_1	58	A_1
144	$A_2 + B_1 + B_2$	143	B_1
		143	A_2
		149	B_2
420	$A_2 + B_1 + B_2$	416	B_2
		417	A_1
		418	B_1
		418	A_2
		423	B_2
		426	A_2

They were unable to distinguish between these, there being no significant difference in the goodness of fit between these space groups. *I*2*cm* is identical to *Ima*2 involving simply a permutation of the *a*, *b*, and *c* axes. The distortion of the lattice that leads to the orthorhombic phase is illustrated in Fig. 4. The oxygen ions move against the Ti ions in the *ab* plane, along the diagonal axis of the octahedra. This Slater-mode-like translation is observed both in the work of Noda *et al.* and also in our calculations.

The phonon modes at the gamma point are Raman active for *Ima*2 and these are collected in Table II. The calculated phonon frequencies and symmetries are in good agreement with the experimental results[34] in almost all cases, particularly for the high-energy modes. The frequencies of the low-energy phonon modes of STO are known to depend strongly on strains present in the crystal,[35] and further, the precision of the phonon calculations in this region is affected by the inaccuracies of cell-shape optimization within DFT. The agreement between the observed and calculated intensities is significantly worse, which may be related to the luminescence present in the experiments, but nevertheless, the overall consistency between our structure C and the available experimental results is good.

An additional way to verify the validity of structure C, without the need for single crystals, might be by the measurement of the difference of the vibrational density of states for the tetragonal (B) and orthorhombic (C) phases. Our calculations predict generally similar profiles, but there is a significant difference between structures B and C at about 60 meV (Fig. 5), which should be observable using inelastic neutron scattering.

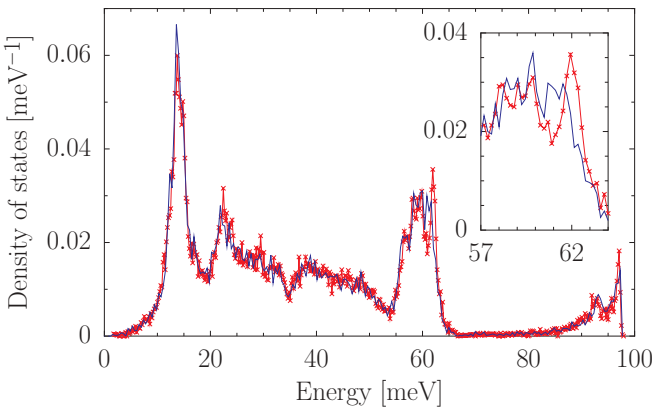

FIG. 5. (Color online) The phonon density of states of $SrTi^{18}O_3$ calculated for (a) tetragonal structure B (blue line) and (b) orthorhombic structure C (red line with crosses). The inset shows the region around 60 meV where the difference between the two is most pronounced.

V. CONCLUSION

Oxygen isotope substitution in STO leads to a ferroelectric phase at low temperatures that we show to occur via a Slater-like phonon mode at the Γ point of the Brillouin zone of the tetragonal, paraelectric phase. Using DFT we determined the structure of the ferroelectric phase of $SrTi^{18}O_3$ to have an orthorhombic unit cell with the *Ima*2 space group, which is noncentrosymmetric and exhibits a ferroelectric moment of (0.57 0 0) eÅ, along the direction that corresponds to [110] in the cubic system.

We have determined the phonon dispersion curves, density of states, and Raman intensities of the proposed ferroelectric phase, and where possible compared these with the existing experimental data. The calculated Raman frequencies are in good agreement with the results published so far and the symmetry of the structure complies with the results of the neutron scattering experiments. Clearly, the most useful experimental data to confirm our results would require fairly large single crystals of STO18 (which are difficult to obtain) for neutron diffraction and the measurement of the dispersion curves.

ACKNOWLEDGMENTS

We would like to thank Ramzi Kutteh for creating the optimized builds of VASP used in our calculations. We thank Yukio Noda and Mitsuru Itoh for a fruitful discussion.

[1] K. A. Müller and H. Burkard, Phys. Rev. B **19**, 3593 (1979).
[2] T. Schneider, H. Beck, and E. Stoll, Phys. Rev. B **13**, 1123 (1976).
[3] J. H. Barrett, Phys. Rev. **86**, 118 (1952).
[4] P. A. Fleury and J. M. Worlock, Phys. Rev. **174**, 613 (1968).
[5] H. Uwe and T. Sakudo, Phys. Rev. B **13**, 271 (1976).
[6] M. Itoh, R. Wang, Y. Inaguma, T. Yamaguchi, Y.-J. Shan, and T. Nakamura, Phys. Rev. Lett. **82**, 3540 (1999).
[7] R. Wang and M. Itoh, Phys. Rev. B **64**, 174104 (2001).
[8] Y. Noda, K. Mochizuki, H. Kimura, M. Itoh, T. Kyomen, and R. Wang, J. Korean Phys. Soc. **46**, 69 (2005).
[9] R. Blinc, B. Zalar, V. V. Laguta, and M. Itoh, Phys. Rev. Lett. **94**, 147601 (2005).
[10] M. Takesada, M. Itoh, and T. Yagi, Phys. Rev. Lett. **96**, 227602 (2006).
[11] M. Takesada, M. Itoh, A. Onodera, and T. Yagi, Ferroelectrics **346**, 20 (2007).
[12] J. C. Slater, Phys. Rev. **78**, 748 (1950).
[13] H. Taniguchi, M. Itoh, and T. Yagi, Phys. Rev. Lett. **99**, 017602 (2007).
[14] H. Taniguchi, T. Yagi, and M. Itoh, Ferroelectrics **369**, 3 (2008).
[15] Y. Uesu, R. Nakai, J.-M. Kiat, C. Ménoret, M. Itoh, and T. Kyomen, J. Phys. Soc. Jpn. **73**, 1139 (2004).
[16] T. Shigenari and K. Abe, Ferroelectrics **369**, 117 (2008).
[17] H. Taniguchi, T. Yagi, M. Takesada, and M. Itoh, Phys. Rev. B **72**, 064111 (2005).
[18] T. Yagi, M. Takesada, H. Taniguchi, and M. Itoh, Ferroelectrics **379**, 168 (2009).
[19] A. Bussmann-Holder, H. Büttner, and A. R. Bishop, Ferroelectrics **363**, 73 (2008).
[20] Y. Yamada, N. Todoroki, and S. Miyashita, Phys. Rev. B **69**, 024103 (2004).
[21] E. Matsushita and S. Segawa, Ferroelectrics **347**, 1 (2007).
[22] Y. Yacoby and Y. Girshberg, Phys. Rev. B **77**, 064116 (2008).
[23] M. Tokunaga and Y. Aikawa, J. Phys. Soc. Jpn. **79**, 024707 (2010).
[24] G. Kresse and J. Furthmüller, Phys. Rev. B **54**, 11169 (1996).
[25] G. Kresse and J. Furthmüller, Comput. Mater. Sci. **6**, 15 (1996).
[26] K. Parlinski, PHONON software, 2003.
[27] P. E. Blöchl, Phys. Rev. B **50**, 17953 (1994).
[28] G. Kresse and D. Joubert, Phys. Rev. B **59**, 1758 (1999).
[29] J. P. Perdew, K. Burke, and M. Ernzerhof, Phys. Rev. Lett. **77**, 3865 (1996).
[30] J. P. Perdew, K. Burke, and M. Ernzerhof, Phys. Rev. Lett. **78**, 1396 (1997).
[31] The direct method (as opposed to linear response, which is implemented in the density functional perturbation theory framework) requires the electronic ground-state calculation to be performed for many copies of the original system, each copy containing an atom displaced from its original position by a small step. The forces acting on atoms in the relaxed structure (in which the atoms are in equilibrium positions in respect to lattice vibrations) are compared with the forces acting on atoms in structures containing displaced atoms. Taking into account the amplitude of the displacement we determine the force constants and resulting dynamic properties of the system within the harmonic approximation. As the harmonic approximation assumes a parabolic potential, a single set of forces corresponding to a displacement of an atom is sufficient to find the shape of the entire potential well in which this atom is located. However, since physical systems are not perfectly harmonic and the potential well is usually asymmetrical (increasing away from the equilibrium position), PHONON allows to derive the result for each direction of displacement from both a positive and negative displacement value to improve the fit of the harmonic model to the properties of the system calculated within DFT. PHONON takes advantage of the symmetry of the system and needs only a minimal set of displacements to find all the elements of dynamical matrix, rather than obtaining the result by displacing every atom in all possible directions.
[32] J. M. Kiat and T. Roisnel, J. Phys. Condens. Matter **8**, 3471 (1996).
[33] T. C. Ozawa and S. J. Kang, J. Appl. Crystallogr. **37**, 679 (2004).
[34] T. Shigenari, K. Abe, T. Takemoto, O. Sanaka, T. Akaike, Y. Sakai, R. Wang, and M. Itoh, Phys. Rev. B **74**, 174121 (2006).
[35] T. Schimizu, Solid State Commun. **102**, 523 (1997).